Induced Smectic-G Phase through Intermolecular Hydrogen Bonding Part VIII: Phase and Crystallization Behaviours of 2-(p-*n*-heptyloxybenzylidene imino)-5-chloro-pyridine: p-*n*-alkoxybenzoic acid (HICP:*n*ABA) Complexes

M. Srinivasulu, P. V. V. Satyanarayana, P. A. Kumar[a], and V. G. K. M. Pisipati[a]

Department of Chemistry, Nagarjuna University, Nagarjuna Nagar 522 510, India
[a] Centre for Liquid Crystal Research and Education, Faculty of Physical Sciences Nagarjuna University, Nagarjuna Nagar 522 510, India

Reprint requests to Prof. V. P.; E-mail: venkata_pisipati@hotmail.com

Z. Naturforsch. **56a,** 685–691 (2001); received June 27, 2001

New intermolecular H-bonded liquid crystalline complexes, viz., 2-(p-*n*-heptyloxybenzylidene imino)-5-chloro-pyridine:p-*n*-alkoxybenzoic acid; (HICP:*n*ABA) (where *n* denotes the alkoxy carbon numbers 3 to 10 and 12) exhibiting smectic-F ($n = 12$) and smectic-G phases have been synthesized and characterized by Thermal Microscopy and Differential Scanning Calorimetry (DSC). Detailed IR (solid and solution states) analysis confirms the existence of intermolecular H-bonding between the pyridyl nitrogen and the COOH group of the p-*n*-alkoxybenzoic acid moiety. The phase behaviour of the series is discussed in the light of reported data on free p-*n*-alkoxybenzoic acids. The crystallization kinetics of a representative complex, using the DSC technique, is discussed. The mechanism of the crystal growth of the new crystalline smectic-G phase is computed with the Avrami equation.

Key words: H-bonding; HICP:*n*ABA; Crystallization Kinetics; Avrami Parameters.

Introduction

In 1989, Kato et al. advanced the concept of H-bonded liquid crystalline materials [1]. In recent years such studies have revived [2–6], as hydrogen bonding, is one of the key interactions producing mesogenic properties [7–10]. Generally, in liquid crystalline systems a homogeneous nucleation process occurs, followed by the sporadic growth of small crystal domains. But in H-bond liquid crystalline systems a different mechanism due to non-covalent interactions is reported [11]. In order to understand such a mechanism, this communication deals with the mesomorphic properties and crystallization kinetics of low molar mass systems, using 2,5-di substituted pyridine as hydrogen bonding acceptor.

Experimental

Materials and Methods

p-*n*-alkoxybenzoic acids (Frinton Laboratories, USA), 2-amino-5-chloro-pyridine (Aldrich), 1-bromo heptane (Aldrich), and p-hydroxy benzaldehyde (Aldrich) were used without further purification. All the other chemicals and solvents were of Analar grade. p-*n*-heptyloxybenzaldehyde was synthesized as reported in [12].

The IR spectra were recorded on a Perkin-Elmer FT-IR (BX series) spectrometer. The liquid crystalline phases and the corresponding transition temperatures were studied by observing the characteristic textures through an Olympus polarizing microscope equipped with a PC based Instec mk1 temperature controller. The enthalpy changes during the phase transitions were determined by a Mettler-Toledo DSC supplemented with an FP-90 central processor. The investigations on crystallization kinetics were performed on a Perkin-Elmer DSC7. The procedure for DSC scans performed at different crystallization temperatures is reported in [13].

2-(p-n-heptyloxybenzylidene imino)-5-chloro-pyridine (HICP)

2-(p-*n*-heptyloxybenzylidene imino)-5-chloro-pyridine (HICP) was prepared [14] by a condensation reaction between the ethanolic solutions (20 ml) of p-*n*-heptyloxybenzaldehyde (3.3 ml/15 mmol) and 2-amino-5-chloro pyridine (1.3 gm/15 mmol) in presence of one or two drops of glacial acetic acid. The white crystalline product obtained on cooling the mixture was recrystallised from a hot methanol solution to get a yield of 3.15 g (63.4%).

0932-0784 / 01 / 0900-0685 $ 06.00

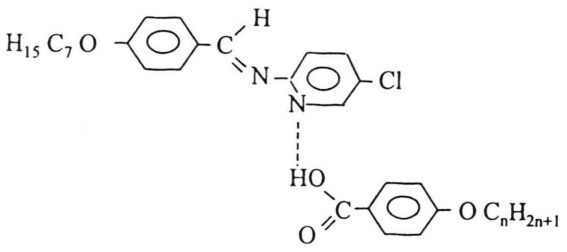

Fig. 1. Molecular structure of 2-(p-*n*-heptyloxybenzylidene imino)-5-chloro-pyridine:p-*n*-alkoxybenzoic acid; (HICP: *n*ABA) complexes.

2-(p-n-heptyloxybenzylidene imino)-5-chloro-pyridine:p-n-alkoxybenzoic acid; (HICP:nABA)

The intermolecular H-bonding complexes of HICP: *n*ABA were synthesized by refluxing equimolar amounts of 2-(p-*n*-heptyloxybenzylidene imino)-5-chloro-pyridine (2.6 g/8 mmol) and p-*n*-alkoxybenzoic acids (8 mmol) in 20 ml of pyridine with constant stirring at 80 °C for ~ 2 h. The excess pyridine was then removed by distillation under reduced pressure. The white crystalline products, obtained after removing the excess pyridine by vacuum distillation, were dried over $CaCl_2$ for ~ 24 h. The crude products were recrystallised from hot dichloromethane solutions to get a yield of 86%. The general molecular formula of the present series of complexes is given in Figure 1.

Results and Discussion

IR Spectra

The IR spectra of p-*n*-alkoxybenzoic acids were recorded at room temperature in both the solid (nujol mull) and solution (chloroform) states. The spectra of free p-*n*-alkoxybenzoic acids showed two sharp bands at 1685 and 1695 cm^{-1} due to the ν(C=O) mode, and a strong band at 3032 cm^{-1}, assigned to the ν(OH) mode of the carboxylic acid group [15]. This doubling of the carbonyl stretching mode may be attributed to the dimeric nature of ABA at room temperature. However, the corresponding spectra recorded in solution (chloroform) show a strong band at 1712 cm^{-1}, suggesting the stabilization of the monomeric form of benzoic acid in solution. To avoid further complications due to such intermolecular interactions, the spectra of complexes were compared with the solution state spectra of free-ABA.

The nujol mull spectrum of the free-HICP moiety exhibits an intense band at ~ 1600 cm^{-1} due to ν(C=O) mode, and two medium intense bands at 669 and 639 cm^{-1} assigned to pyridine ring deformation modes. However, the infrared frequencies of HICP:*n*ABA show a sharp band at ~ 1680 cm^{-1} due to the ν(C=O) mode of the benzoic acid moiety, which suggests the monomeric nature upon complexation. When compared with the free-ABA spectra, the HICP:*n*ABA complexes show bathochromic shifts (~ 30 cm^{-1}) in the ν(C=O) mode of the acid, and hypsochromic shifts (~ 50 cm^{-1}) in the pyridine ring deformation modes of HICP moiety. This strongly suggests the formation of intermolecular hydrogen bonding between the COOH group of ABA and the pyridine ring nitrogen of HICP. Moreover, the band associated with the ν(OH) mode of the carboxylic acid group suffered a hypsochromic shift upon complexation, which strongly supports the existence of H-bonding. The presence of intermolecular H-bonding is further invoked by the appearance of a new band with medium intensity at ~ 2920 cm^{-1}, diagnostic of the ν(H----N) mode [15, 16] in all compounds of the present series.

The degree of stabilization of intermolecular hydrogen bonding was further studied by recording the spectra of the complexes in chloroform solution. The spectra show the reappearance of the doubling nature in the stretching modes of free p-*n*-alkoxybenzoic acids and the deformation modes of the free-pyridine ring moiety. This, however, clearly implies the destruction of intermolecular H-bonding in the solution state.

Thermal and Phase Behaviour

The phase variants and transition temperatures of free p-*n*-alkoxybenzoic acids (*n*ABA) and the corresponding series of intermolecular hydrogen bonded complexes are determined from the characteristic [17] textural observations using a polarizing microscope at a scan rate of 0.1 °C per minute. The temperatures of the corresponding phase transitions and their heats of transition (in joules per gram) were further measured using differential scanning calorimetry (DSC) at a scan rate of 5 °C per minute. The transition temperatures from thermal microscopy (TM) and DSC along with the enthalpy values for the present series of complexes are given in Table 1. Results pertaining to the phase behaviour of the H-bonded complexes in conjunction with free p-*n*-alkoxy benzoic acids are discussed below.

Table 1. Transition temperatures (°C) from TM and DSC for HICP:*n*ABA complexes. Enthalpy values are given in parenthesis. (N = nematic, C = smectic C, F = smectic-F, G = smectic G).

Complex[#]	Phase variant	Phase transition temperatures/°C from TM and DSC (ΔH J/g)				
		Iso.-N/G	N–C/G	C–F/G	F–G	G–Cryst.
I	G	121.4 [120.1 (22.8)]				98.0 [97.2 (21.2)]
II	G	136.1 [135.0 (17.9)]				84.6 [85.7 ([a])]
III	NG	121.0 [120.5 (0.3)]	106.7 [105.9 (6.1)]			83.2 [82.4 ([a])]
IV	NG	143.1 [142.0 (0.5)]	106.6 [101.4 (*)]			81.1 [84.4 (14.2)]
V	NG	134.6 [134.0 (0.6)]	106.2 [104.5 (8.1)]			78.9 [77.8 (9.7)]
VI	NCG	126.7 [124.5 (0.5)]	113.6 [114.0 (0.4)]	85.0 [85.8 (26.7)]		45.1 [44.3 (42.1)]
VII	NCG	135.4 [135.0 (0.2)]	92.1 [90.8 (*)]	80.7 [78.8 (4.1)]		63.4 [54.9 (53.3)]
VIII	NCG	130.0 [128.0 (0.4)]	109.2 [110.4 (1.9)]	84.1 [83.6 (21.0)]		74.1 [73.8 (17.4)]
IX	NCFG	132.8 [132.2 (0.2)]	104.7 [105.0 (*)]	94.2 [93.4 (4.4)]	78.8 [77.9 (14.2)]	67.1 [68.1 (6.8)]

[#] I–IX represent alkyl chain lengths of ABA: propyl-, butyl, pentyl-, hexyl-, heptyl-, octyl-, nonyl-, decyl-, and dodecyl-, respectively.
* Transition peaks are not well resolved. [a] DSC peak is not observed.

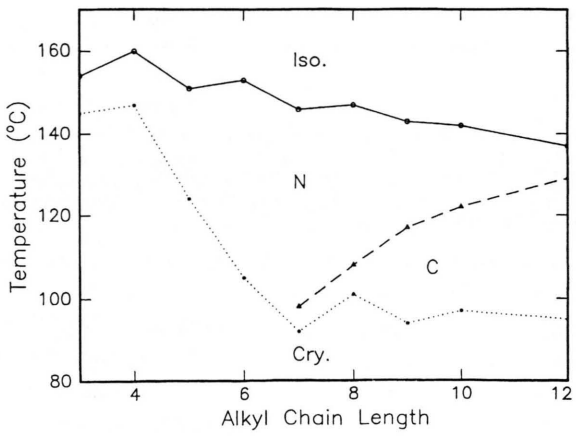

Fig. 2. Phase diagram of p-*n*-alkoxybenzoic acids. (N = nematic, C = smectic C).

Microscopic observations reveal that the lower homologues (n = 3 to 6) p-*n*-alkoxybenzoic acids exhibit a nematic (marble) mesophase, and the higher members of the series a smectic-C (schlieren) phase [3]. The phase transition temperatures observed through thermal microscopy are in reasonable agreement with the corresponding DSC data. The general phase behaviour of *n*ABA is depicted in Figure 2. The thermal distribution of the smectic-C phase increases with simultaneous quenching of the nematic phase [3, 8] with increase of the alkoxy carbon number of the benzoic acids.

On cooling the isotropic melt, the HICP:*n*ABA series exhibits nematic (n = 5 to 12), smectic-C (n = 8 to 12), smectic-F (n = 12) and smectic-G (all complexes) phases. The formation of the nematic phase begins with small droplets, which on further cooling leads to the formation of a four-brush schlieren texture. The transition from the nematic to the smectic-C phase is characterized by the appearance of a two-brush schlieren texture. On further cooling, the complex IX shows the appearance of a broken focal conic fan texture, which is assigned to the transition from the smectic-C to the smectic-F phase. In all complexes of this series, formation of the smectic-G phase is observed as a smooth multicoloured mosaic texture. The phase transition temperatures observed by thermal microscopy and from DSC data agree reasonably (Table 1).

Figure 3 summarizes the thermal and phase behaviour of the present series with respect to its analogue members of the free-*n*ABA series. This phase diagram

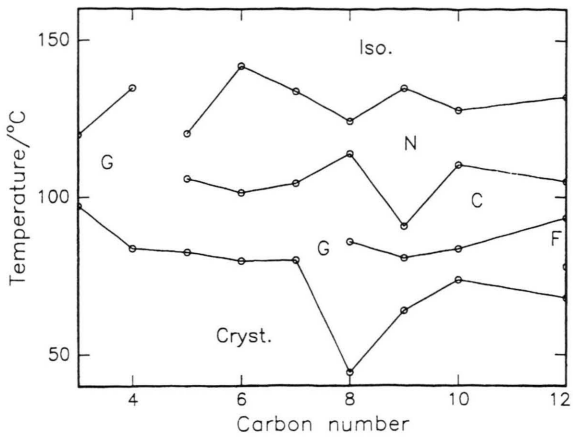

Fig. 3. Phase diagram of 2-(p-*n*-heptyloxybenzylidene imino)-5-chloro-pyridine:p-*n*-alkoxybenzoic acid; (HICP:*n*ABA) complexes. (N = nematic, C = smectic C, G = smectic G).

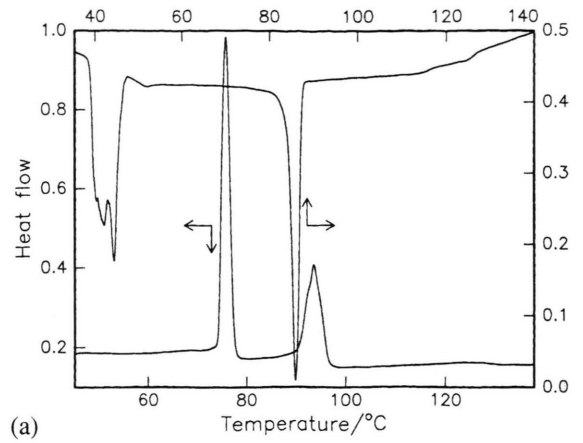

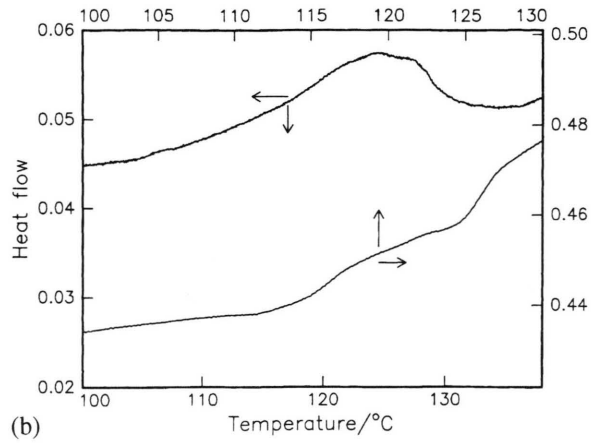

Fig. 4. DSC thermograms of (a) 2-(p-*n*-heptyloxybenzylidene imino)-5-chloro-pyridine:p-*n*-octyloxybenzoic acid; (HICP:*n*OBA) complex (38–140 °C). (b) 2-(p-*n*-heptyloxybenzylidene imino)-5-chloro-pyridine:p-*n*-octyloxybenzoic acid; (HICP:*n*OBA) complex (100–140 °C).

shows a different trend in this series. The striking feature is the induction of tilted phases, smectic-G (in all the members) and smectic-F (carbon number = 12) phases. The inducement of a new phase variant, isotropic to smectic-G, is observed for the complexes I and II, and a sudden appearance of the nematic phase is noticed in the complexes III to IX. For the lower homologues (n = 5 to 7), the nematic and smectic-G phases are dominant, while the thermal ranges of the smectic-C and smectic-G phases are equally distributed among the higher homologues. Note that the complex IX exhibits a phase variant of NCFG. Note also that a maximum thermal distribution of the induced phase (Sm-G) is found in complexes that contain butyl- and octyl- carbon chains. A noteworthy feature in the phase behaviour of the higher homologues (Fig. 3) is the stabilization of the smectic-C phase. The liquid crystalline thermal range of the present series is larger than that of the free-*n*ABA series. However, the overall transition temperatures of the series also show an odd-even effect.

Crystallization Kinetics

2-(p-n-heptyloxybenzylidene imino)-5-chloro-pyridine:p-n-alkoxybenzoic acid; (HICP:nOBA)

Crystallization Temperatures

DSC thermograms of HICP:*n*OBA in heating and cooling cycles are summarized in Figure 4. The heating scan shows three pertinent transitions at 76.0, 93.7 and 126.7 °C with the corresponding enthalpies 37.8, 21.4 and 0.8 J/g, which are assigned to the transitions, crystal to melting, smectic-G to nematic, and nematic to isotropic, respectively. On cooling the sample from its isotropic melt, the compound exhibits the transitions isotropic to nematic (124.5 °C), nematic to smectic-C (114.0 °C), smectic-C to smectic-G (85.8 °C) and smectic-G to crystal (44.3 °C) with the corresponding enthalpies 0.5, 0.4, 26.7 and 42.1 J/g, respectively. As borne out by the thermal range between the melting and crystal exotherms, the crystallization kinetics relating to the transition from the smectic-G phase is selectively performed at the crystallization temperatures,

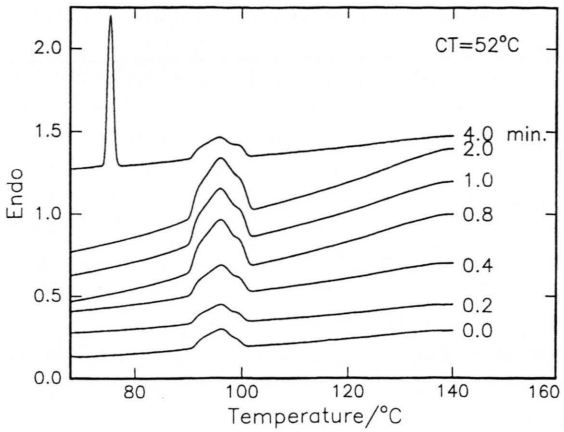

Fig. 5. DSC endotherm profiles of 2-(p-*n*-heptyloxybenzylidene imino)-5-chloro-pyridine:p-*n*-octyloxybenzoic acid; (HICP:*n*OBA) complex at 52 °C for different time intervals. CT = crystallization temperature.

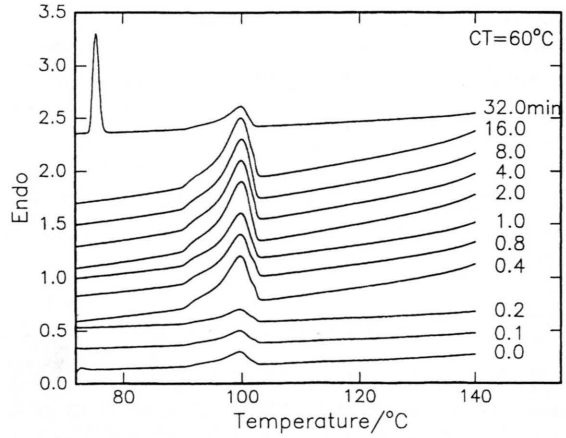

Fig. 6. DSC endotherm profiles of 2-(p-*n*-heptyloxybenzylidene imino)-5-chloro-pyridine:p-*n*-octyloxybenzoic acid; (HICP:*n*OBA) complex at 60 °C for different time intervals. CT = crystallization temperature.

52, 54, 56, 58 and 60 °C. Typical endotherm profiles for different time intervals at the crystallization temperatures 52 and 60 °C are represented in Figs. 5 and 6, respectively.

Rate of Crystallization

The compound is held at an initial crystallization temperature, 52 °C, for different time intervals (0.2 to 4.0 minutes). The heating curves, recorded after holding the compound for time intervals of 0.2 to 2.0 minutes, displays smectic-G to nematic and nematic to isotropic transitions, indicating the non-existence of a crystal to melting transition. Interestingly, after holding the sample for 4.0 minutes the sudden appearance of a crystal to melting transition with a saturated value of enthalpy clearly suggests a fast crystallization process. The trend in the growth of this melting transition exactly resembles the reported [11] one of the 2,2′-bipyridine:p-*n*-octyloxybenzoic acid (BP:OBA) complex. The kinetic experiments at different crystallization temperatures also indicate the similar trend of nucleation behaviour associated with the melting transition.

In order to show the role of the alkoxy chain length of the pyridyl moiety on the rate of crystallization we made a comparison with the reported [2] series of complexes, 2-(p-*n*-nonyloxybenzylidene imino)-5-chloro-pyridine:p-*n*-alkoxybenzoic acid; (NICP:*n*ABA) which clearly suggested a different crystallization behaviour. At the final crystallization temperature, NICP:*n*ABA exhibited slow crystallization within 240 min. This clearly shows the role of the alkoxy chain length of the pyridyl moiety on the crystallization behaviour.

Avrami Parameters

It is known that crystallization processes involving the fraction of the transformed volume, x at a time t, measured since the beginning of the crystallization, are described [18, 19] by the Avrami equation

$$x = 1 - \exp(-bt^n), \tag{1}$$

where the constant b and n depend on the nucleation mechanism and the geometry of the growing domains, respectively. x at t is given by $\Delta H/\Delta H_0$, where ΔH is the melting heat measured at the time t, and ΔH_0 is the maximum value obtained from the plateau of individual master curves.

If the crystallization kinetics of the corresponding smectic phases are described by the above Avrami equation, the data for all the crystallization temperatures will match the equation [20]

$$x = 1 - \exp\{-(t/t^*)^n\}, \tag{2}$$

where $t^* = b^{-1/n}$. Further, the characteristic time t^* can be experimentally determined, since at $t = t^*$, $x = 0.632$. Substituting these values of t^* and x in (1), the constants b and n for a specified crystallization temperature are obtained.

Table 2. Crystallization parameters measured in the smectic-G phase of HICP:*n*ABA complexes.

Compound	Crystallization temperature/°C	t^*/min.	x	n	b
HICP:OBA	52	4.0	0.9626	0.822	3.0×10^{-1}
	54	4.0	0.9679	0.860	2.9×10^{-1}
	56	32.0	0.9915	0.149	2.1×10^{-1}
	58	32.0	1.0000	0.541	0.6×10^{-1}
	60	32.0	0.9964	0.176	1.8×10^{-1}

The Transformed Volume x

In general, a phase transition from one distinct phase to another may be considered as the transformation from one completely ordered phase to another completely ordered phase. During such a transition, however, the co-existence of phases in each other's matrix may look like a disordered phase. Thus, the process of transformation consists of the growth of one species at the expense of the other, passing through a state of maximum disorder. The transformation from phase I to phase II can be considered as occurring by two routes: (a) *nucleation* which involves a spontaneous conversion of some isolated units of phase I into phase II when it is not surrounded by II and (b) *propagation step* ascribed to the conversion of phase I to phase II at I–II interfaces, where the activation energy for conversion is likely to be low. Nevertheless, both these nucleation and propagation steps are solely dependent upon nucleation and growth rates. As the phase II grows inside the matrix of phase I, the growth continues until phase-I impinges on a growth barrier like domains or free surfaces. Thus, the total rate may be written as dx/dt, where x is the fraction of phase I which has transformed into phase II in the time t. At this juncture, if the nucleation and the growth rates are combined with due correction for impingement of transformed domains, the total transformed volume of a given phase will become equal to f(t).

In the present investigation the transformed volume, x at a particular crystallization time, is deduced from the experimental data of $\Delta H/\Delta H_0$, (Table 2). It is found that the magnitude of x reaches unity at high crystallization temperatures with a delayed crystallization time (~ 32 min).

The Dimensionality Parameter n

It is well known that the Avrami exponent n plays a crucial role in ascertaining the mode and class of rate transformations which occur when a stable low temperature phase growth out of a mother metastable phase in the form of small domains [21]. It is observed that in diffusionless or polymorphic or cellular transformations, if $n > 3$, then the crystal nucleation occurs either at a constant rate or increasing rate. For $n = 3$, the nucleation occurs only at the start of the transformation. The latter continues to the grain edges or boundaries when the magnitude of n reaches to < 3. On the other hand, the lower values of n(0.5 to 2.5) favour the diffusion-controlled transformations in which the nucleation starts as an initial growth of particles in the form of plates or needles of finite size possessing impinged edges.

The values of n, calculated for HICP:OBA from (2) for different crystallization temperatures, vary between 0.15 and 0.86 (Table 2). The low values may be assigned to the occurrence of diffusion-controlled transformations involving the formation of finite size plates or needles [21]. A sudden decrease in the Avrami exponent is observed at the crystallization temperature, 56 °C. This supports the occurrence of nucleation growth that facilitates the thickening of plates at the micro level and promotes a delayed kinetics process. This observation is, however, inconsistent with the delayed crystallization time (t^* = 32.0 minutes) at the same crystallization temperature. The data also support the existence of a two-dimensional sporadic nucleation growth [21].

The Nucleation Growth Parameter b

The constant b, which governs the nucleation mechanism, is of the order of 10^{-1}. Its trend is in good agreement with the reported data for NICP:*n*ABA, DBA:ACP and BP:OBA [2, 4, 11].

Conclusion

The thermal and phase studies on the present series reveal in the inducement of tilted phases (Smectic-F, smectic-G) with simultaneous quenching of nematic (in lower homologue) and smectic-C (in middle members) phases, when compared to free-ABA. The induction of these tilted phases may best be interpreted in terms of possible molecular contributions originating from the intermolecular H-bonding between the electron rich hetero atom (nitrogen) and an acid group. Apart from this non-covalent interaction, the tendency of perma-

nent transverse dipole (viz., chlorine) in delocalizing the electron cloud may also have a significant role towards the origin of the new phases. The detailed IR structural study confirmes the existence of hydrogen bonds between the pyridine ring nitrogen of HICP and the COOH group of ABA.

The kinetics studies performed on a representative compound reveal an altogether different trend of crystallization behaviour. A sudden growth of melting transition is observed after the completion of the final characteristic time interval at each crystallization temperature. The effective role of the alkoxy chain length on the crystallization rate is realized by a relatively slow crystallization rate of HICP:OBA when compared to its reported analogous series. Moreover, the value of dimensionality parameter n varies for each crystallization temperature, which in turn suggests an independent nucleation mechanism. A possible explanation towards this crystallization behavior can be accounted on the basis of sporadic nucleation growth, which follows an inhomogeneous process of continuous nucleation over a constant time. It is reasonable to conclude that the strength of hydrogen bonds at a particular crystallization temperature plays a dominating role on the crystallization time. Nevertheless, the proton donor and acceptor capabilities of the pyridine nitrogen and acid group may also have a profound influence on the over all crystallization mechanism.

Acknowledgements

Authors express their appreciation to Prof. K. G. Subhadra of Kakatiya University, Warangal, India for IR spectral recording. M. S. and P. A. K. acknowledge the financial assistance rendered by the Council of Scientific and Industrial Research (CSIR). Thanks are also due to the University Grants Commission (UGC) under DRS scheme and the Department of Science and Technology (DST), New Delhi, for financial support.

[1] T. Kato and M. J. Frechet, J. Amer. Chem. Soc. **11,** 8533 (1989).
[2] M. Srinivasulu, P. V. V. Satyanarayana, P. A. Kumar, and V. G. K. M. Pisipati, Mol. Mater. (2001) in press.
[3] P. A. Kumar, M. Srinivasulu, and V. G. K. M. Pisipati, Liq. Cryst. **26,** 1339 (1999).
[4] P. Swathi, P. A. Kumar, and V. G. K. M. Pisipati, Liq. Cryst. (2001) accepted.
[5] P. Swathi, S. Sreehari Sastry, P. A. Kumar, and V. G. K. M. Pisipati, Mol. Cryst. Liq. Cryst. (2001) in press.
[6] E. B. Barmatov, A. Yu, Bobrovsky, M. V. Barmatova, and V. P. Shibaev, Liq. Cryst. **26,** 581 (1999).
[7] Min Li, Hongjin Qiu, Xinfang Chen, Gao Li, and Enle Zhou, Liq. Cryst. **26,** 1053 (1999).
[8] Z. Sideratov, Tsiourvasd., C. M. Paleos, and A. Skoulios, Liq. Cryst. **22,** 51 (1997).
[9] T. Kato and M. J. Frechet, Macromol. Symp. **98,** 311 (1995).
[10] T. Kato and M. J. Frechet, Macromolecules **22,** 3818 (1989).
[11] M. Srinivasulu, P. V. V. Satyanarayana, P. A. Kumar, and V. G. K. M. Pisipati, Liq. Cryst. **28,** (2001) in press.
[12] P. Keller and L. Liebert, Solid State Physics, supplement **14,** 19–76 (Academic Press Inc.) (1978).
[13] P. A. Kumar, M. L. N. Madhu Mohan, and V. G. K. M. Pisipati, Liq. Cryst **27,** 727 (2000).
[14] N. V. S. Rao and V. G. K. M. Pisipati, Phase Trans. **3,** 317 (1983).
[15] K. Nakamoto, Infrared and Raman Spectra of Inorganic and Coordination compounds, 4th ed., Interscience New York 1978.
[16] Addison Ault., Techniques and Experiments for Organic Chemistry, 3rd ed., Allen and Bacon Inc., New York 1979.
[17] G. W. Gray and J. W. G. Goodby, Smectic Liquid Crystals: Textures and Structures, Leonard Hill, London 1984.
[18] M. Avrami, J. Chem. Phys. **7,** 1103 (1939).
[19] M. Avrami, J. Chem. Phys. **8,** 212 (1939).
[20] Ziru He, Yue Zhao, and Caille Alain, Liq. Cryst. **23,** 317 (1997).
[21] C. N. R. Rao and K. J. Rao, Phase Transitions in Solids, Mc. Graw-Hill, New York 1978.